

Magnetic Resonance Imaging of Vascular Oxygenation Changes during Hyperoxia and Carbogen Challenges in the Human Retina

Yi Zhang,^{1,2,3} Qi Peng,^{1,2,3} Jeffrey W. Kiel,⁴ Carlos A. Rosende,⁴
and Timothy Q. Duong^{1,2,4,5,6}

PURPOSE. To demonstrate blood oxygenation level-dependent (BOLD) magnetic resonance imaging (MRI) of vascular oxygenation changes in normal, unanesthetized human retinas associated with oxygen and carbogen challenge.

METHODS. MRI was performed with a 3-T human scanner and a custom-made surface-coil detector on normal volunteers. BOLD MRI with inversion recovery was used to suppress the vitreous signal. During MRI measurements, volunteers underwent three episodes of air and 100% oxygen or carbogen (5% CO₂ and 95% O₂) breathing. Eye movement was effectively managed with eye fixation, synchronized blinks, and postprocessing image coregistration. BOLD time-series images were analyzed using the cross-correlation method. Percent changes due to oxygen or carbogen inhalation versus air were tabulated for whole-retina and different regions of the retina.

RESULTS. Robust BOLD responses were detected. BOLD MRI percent change from a large region of interest at the posterior pole of the retina was $5.2 \pm 1.5\%$ ($N = 9$ trials from five subjects) for oxygen inhalation and $5.2 \pm 1.3\%$ ($N = 11$ trials from five subjects) for carbogen inhalation. Group-averaged BOLD percent changes were not significantly different between oxygen and carbogen challenges ($P > 0.05$). The foveal region had greater BOLD response compared with the optic nerve head region for both challenges.

CONCLUSIONS. BOLD retinal responses to oxygen and carbogen breathing in unanesthetized humans can be reliably imaged at high spatiotemporal resolution. BOLD MRI has the potential to provide a valuable tool to study retinal physiology and pathophysiology, such as how vascular oxygenation at the tissue level is regulated in the normal retina, and how retinal diseases may affect oxygen response. (*Invest Ophthalmol Vis Sci.* 2011; 52:286–291) DOI:10.1167/iovs.10-6108

From the ¹Research Imaging Institute and the Departments of ²Radiology, ⁴Ophthalmology, and ⁵Physiology, University of Texas Health Science Center, San Antonio, Texas; and ⁶South Texas Veterans Health Care System, San Antonio, Texas.

³Contributed equally to the work and therefore should be considered equivalent authors.

Supported by a Pilot grant (TQD); a Translational Technology Resource grant (QP) via the Clinical Translational Science Award (CTSA, parent Grant UL1RR025767); the NIH/NEI (R01 EY014211 and EY018855 to TQD); and the VISN7 Career Development Award and MERIT from the Department of Veterans Affairs (TQD).

Submitted for publication June 23, 2010; revised August 11, 2010; accepted August 11, 2010.

Disclosure: Y. Zhang, None; Q. Peng, None; J.W. Kiel, None; C.A. Rosende, None; T.Q. Duong, None

Corresponding author: Timothy Q. Duong, University of Texas Health Science Center at San Antonio, Research Imaging Institute, 8403 Floyd Curl Drive, San Antonio, TX 78229; duongt@uthscsa.edu.

The retina provides the first stage of visual processing. Many blinding diseases—including diabetic retinopathy, glaucoma, macular degeneration, and retinitis pigmentosa—affect predominantly the retina. Loss of vision severely affects patient quality of life. Imaging modalities that provide early detection and improve understanding of retinal disease pathophysiology offer the potential to improve treatment outcomes and facilitate development and monitoring of therapeutic interventions. Patients at risk can be managed more aggressively and are more likely to follow treatment regimens diligently.

Optical imaging techniques have been used historically to study the retina. These include optical coherence tomography¹ for imaging fundus anatomy, life-time phosphorescent imaging² and spectral reflectance^{3–5} for detecting oxygenation changes, fluorescein angiography,⁶ indocyanine-green angiography,⁷ scanning laser ophthalmoscopy,⁸ laser Doppler velocimetry⁹ and flowmetry,^{10,11} and laser speckle flowgraphy^{12,13} for measuring blood flow or velocity. Functional imaging associated with visual stimulation has been recently reported using intrinsic optical imaging^{3–5} and laser Doppler flowmetry.^{14,15} With the exception of optical coherence tomography for anatomical imaging, optical techniques have ambiguous depth resolution. These techniques are also hindered by opacities in the vitreous humor, cornea, or lens (such as vitreal hemorrhage and cataract).

In contrast, magnetic resonance imaging (MRI) has no depth limitation and a large field of view and is widely used to noninvasively image anatomy, physiology, and function of the brain in both research and clinical settings. In particular, blood oxygenation level-dependent (BOLD) MRI,^{16,17} in which the signal contrast originates from the intravoxel magnetic field inhomogeneity induced by paramagnetic deoxyhemoglobin in the erythrocytes in blood, offers a valuable method to measure vascular oxygenation changes noninvasively and has been widely used to study brain function physiology in normal and diseased states. Although the current spatial resolution of MRI is lower than optical techniques, recent advances have made it possible to achieve high-resolution functional MRI (fMRI) of columnar^{18–20} and laminar structures^{21,22} in the brain of humans and animals. MRI applications in retinas have also been recently reported in anesthetized animal models. Retinal anatomical laminar resolution,^{23,24} relaxation and diffusion time constants,^{23,25,26} manganese-enhanced MRI,²⁷ blood flow MRI,^{28–30} blood volume,³¹ and BOLD MRI during physiological²⁴ and visual stimuli³² in animal models are becoming feasible.

MRI applications to the human retina, however, face several additional challenges compared with anesthetized animals for three reasons: (1) clinical magnetic field gradients are less powerful compared with those on animal scanners, limiting spatial resolution; (2) the capability to optimize field homogeneity by shimming on clinical scanners is also less powerful

compared with those on animal scanners, which can result in magnetic susceptibility artifacts such as signal dropout and image distortion in regions close to air-tissue interface; and (3) eye motion in unanesthetized humans can hamper time-series fMRI investigation of the retina. Consequently, there is a paucity of MRI applications in the unanesthetized human retina. Nevertheless, a high-resolution anatomic MRI study of the eye³³ and a blood flow MRI of the human retina in a conference abstract³⁴ have been reported.

The purpose of this study was to demonstrate the feasibility of a novel BOLD fMRI application associated with oxygen and carbogen (5% CO₂ and 95% O₂) inhalation in the normal unanesthetized human retina. BOLD fMRI used an inversion-recovery principles of echo shifting using a train of observations (IR-PRESTO) pulse sequence³⁵ to minimize image distortion and signal dropout in the region of the eye where magnetic susceptibility variation is high. Inversion-recovery contrast was used to suppress the vitreous signal and to minimize the partial volume effect (PVE) from the vitreous and sclera that surround the retina. The size, shape, and position of the custom-made surface coil were carefully chosen to optimize the signal-to-noise ratio (SNR) at the posterior pole of the retina. Strategies to minimize eye motion and susceptibility artifacts, postprocessing image coregistration, and reproducibility of BOLD fMRI measurements were also evaluated. This approach has the potential to offer unique and important physiological imaging data without depth limitation that could complement existing retinal imaging techniques.

METHODS

MR Protocol

Multiple studies were performed on five normal human volunteers (one female and four males, 22 to 35 years old) with approval of the Institutional Review Board. All subjects were treated in accordance with the Declaration of Helsinki. Two to three repeated experiments were performed on different days on each subject. To minimize eye motion during active MRI scans, subjects were instructed to blink, if needed, only immediately after the data readout train (which generated distinct sounds as a cue) but otherwise maintain binocular fixation on a point in the scanner.

MRI was performed on a 3-T whole-body MR scanner (Achieva, Philips Health care, Best, The Netherlands). A custom-made head-holder was used to minimize gross head motion. The standard whole-body quadrature radio frequency (RF) coil was used for excitation. A custom-made, oval-shaped, receive-only eye coil of 5 × 7 cm diameter was mounted on a pair of swimming goggles. The size of the coil was optimized for SNR in the central region of the human retina (~3 cm deep from the corneal surface). The right eye was evaluated in all subjects, and a single axial slice bisecting the center of the lens and the optic nerve head was chosen for BOLD MRI analysis. Care was taken to choose a similar MRI slice with similar orientation within and across subjects. Position was verified before each fMRI trial by an anatomic localizer. Magnetic field homogeneity was optimized by local high-order shimming of the posterior part of the eye centered at the retina (shimming volume 2.5 × 2.5 × 1.0 cm).

BOLD fMRI scans used a two-dimensional IR-PRESTO sequence³⁵ with repetition cycle between inversion pulses of 4000 ms and inversion delay of 1300 ms. Inversion recovery procedure was applied to suppress the otherwise bright vitreous signal. Other MRI parameters were repetition time (TR) = 11 ms, echo time (TE) = 17 ms, flip angle (FA) = 10°, readout bandwidth = 6.4 kHz, FOV = 100 × 100 mm, matrix size = 64 × 50, and spatial resolution of 1.6 × 2 × 4 mm. The higher resolution direction was placed along the anterior-posterior direction. A relatively short echo time was chosen to compensate for imaging in a region of large magnetic susceptibility variation. The temporal resolution per image was 4 seconds.

Gas Challenges

BOLD fMRI results were acquired during three repeated episodes of breathing 100% oxygen or carbogen (5% CO₂ + 95% O₂) for 40 seconds followed by air breathing for 80 seconds. Gas, flowing at ~11 L/min, was delivered via an inhalation face mask. The total scan duration for each trial was 7 minutes and 20 seconds. A break of 5 to 10 minutes was given between trials.

Data Analysis

Time-series movies of MR images were evaluated to ensure the absence of gross motion or large fluctuations of signal intensity. MR images in the time series were coregistered. BOLD fMRI time-series images were analyzed using cross-correlation methods (FMRIB's Software Library). A background signal intensity threshold was applied to exclude low-intensity pixels (such as noisy background and the suppressed vitreous) from fMRI analysis.

Statistical *z*-score maps were calculated (without correcting for temporal smoothing). All time courses had bandpass temporal smoothing (range, 0.008~0.125 Hz). Percent changes due to oxygen and carbogen inhalation were obtained with 90% of maximum signal changes as commonly used. Percent changes were tabulated for "activated[b]" pixels (*z*-score > 1.6) from a large region of interest (ROI) encompassing the posterior part of retina (see image inset in Figs. 1B and 2B). To evaluate regional variation of the BOLD responses, the posterior retina was segmented into four equal regions (see Fig. 4) including the fovea (region 2) and optic nerve head (region 3) as well as their neighboring regions. Region 3 was centered at the optic nerve head. The length of each segment along the retina was 3.5 mm. Regional percent changes were tabulated for the entire segmented ROIs.

Statistical Analysis

Data from individual trials were analyzed. Statistical analysis was performed across trials. Values and error bars are mean ± SD. Statistical tests for differences between oxygen and carbogen challenges used unpaired *t*-tests. Statistical tests among different regions within the retinas used one-way ANOVA and Tukey's honestly significant difference test. *P* < 0.05 was taken to be statistically significant.

RESULTS

The size and curvature of the custom-built, receive-only RF coil—mounted onto a swimming goggle—were carefully optimized for SNR at the posterior part of the retina. Mounting the RF coil onto the goggle offered comfort, stability, and consistency.

Conventional gradient-echo echo-planar-imaging BOLD fMRI with single-, two-, and four-shot acquisitions were explored but yielded unacceptable susceptibility artifacts and signal dropout (data not shown). PRESTO acquisition overcame these limitations while maintaining high spatiotemporal resolution.

With eye fixation and blink immediately after data acquisition, none of the subjects reported any significant discomfort. BOLD fMRI time-series images of the retina were free of movement artifacts. Time-series movies of the MR images showed no gross motion. Infrequent drift and minor movement were readily corrected. Figure 1 shows a BOLD fMRI color activation map overlaid on the T2*-weighted image and the corresponding time course associated with oxygen challenge from a representative subject with a spatial resolution of 1.6 × 2 × 4 mm and the temporal resolution of 4 seconds per time point. The T2*-weighted image showed no significant image distortion or signal dropout. BOLD fMRI responses to oxygen inhalation were reliably detected to be highly localized to the retina as well as the optic nerve and the surrounding tissue. No signal

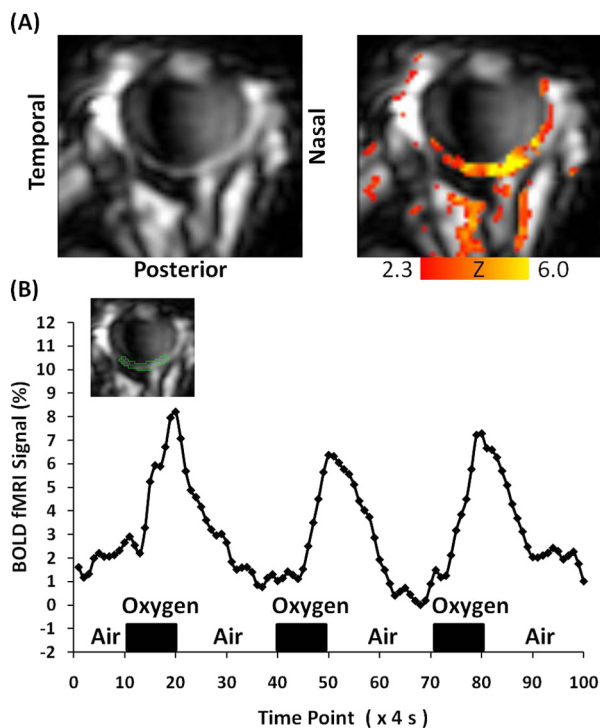


FIGURE 1. BOLD fMRI (A) color activation map and (B) time course associated with oxygen challenge versus air from a representative subject. The background image was a single scan. MRI parameters: inversion-recovery PRESTO image with FA = 10°, TR/TE = 11/17 ms, spatial resolution = $1.6 \times 2 \times 4$ mm, and inversion delay 1300 ms.

changes were detected in the lens and vitreous except a few scatter pixels. To avoid bias, MRI time courses were obtained from an ROI of the posterior part of the retina (as indicated on the inset image). BOLD signal temporal responses to oxygen inhalation were observed. The group-averaged BOLD increase during oxygen challenge was $5.2 \pm 1.5\%$ ($N = 9$ independent trials from five subjects).

Similarly, Figure 2 shows a BOLD fMRI color activation map and the corresponding time course associated with carbogen challenge from a representative subject. BOLD fMRI responses to carbogen inhalation were also reliably detected and localized to the retina as well as the optic nerve and the surrounding tissue. Similarly, no signal changes were detected in the anterior chamber, lens, and vitreous. The group-averaged BOLD percent changes to carbogen challenge were $5.2 \pm 1.3\%$ ($N = 11$ trials from five subjects). The group-averaged percent changes from carbogen challenge were not statistically different from those from oxygen challenge ($P > 0.05$).

Figure 3 shows a reproducibility test of BOLD fMRI color activation maps associated with carbogen challenge of three repeated trials from the same representative subject in the same setting. The reproducibility index referred to the mean and standard deviations computed for three repeated measurements. The activation patterns in the retina were reasonably reproducible. The ROI (as indicated on the inset image) BOLD percent changes ($6.2 \pm 1.2\%$, $4.9 \pm 0.9\%$, and $4.4 \pm 1.0\%$, where the standard deviations were those across pixels within the ROI) were also reasonably reproducible.

Regional fMRI responses of the four ROIs in the retina are shown in Figure 4. The percent changes between oxygen and carbogen challenges were not statistically different from each other in any of the ROIs ($P > 0.05$). For oxygen challenges, percent changes were statistically different between region 1 and 4, between 2 and 3, and between 2 and 4 ($P < 0.01$). For

carbogen challenges, percent changes were statistically different between regions 2 and 4 ($P < 0.05$) and between regions 2 and 3 ($P < 0.01$).

DISCUSSION

This study demonstrates, for the first time, a novel MRI application to detect BOLD fMRI signal changes associated with oxygen and carbogen challenges in the unanesthetized human retina without depth limitation at reasonably high spatiotemporal resolution on a clinical 3 T scanner. These findings indicate that clinical scanners have sufficient SNR, gradient strength, and stability to perform retinal BOLD fMRI in unanesthetized humans. This was made possible by optimizing a custom-designed eye coil and the MRI sequence and sequence parameters so that they are free of susceptibility artifacts. Eye movement can be effectively managed with eye fixation, synchronized blinks, and postprocessing image coregistration. BOLD fMRI has the potential to provide a valuable tool to study retinal physiology and pathophysiology, including how vascular oxygenation is regulated at the tissue level in the normal retina in vivo, and how retinal diseases may affect oxygen response in the retina. This study provides encouraging data to further explore BOLD fMRI of the retina in unanesthetized humans. Additional improvement in spatial resolution and sensitivity is expected.

The unique advantages of BOLD fMRI include depth resolution, images unhindered by media opacity, and a large field of view, compared with many optically based imaging techniques. The disadvantages of BOLD fMRI include poorer spatiotemporal resolution compared with optically based imaging techniques. The need for adequate eye fixation, particularly in some patients with eye diseases, may limit BOLD fMRI application to the retina. BOLD fMRI measures relative oxygenation changes (i.e., not quantitative) because BOLD signals are difficult to quantify given the confounds by many physiological and measurement parameters. Nonetheless, BOLD fMRI could pro-

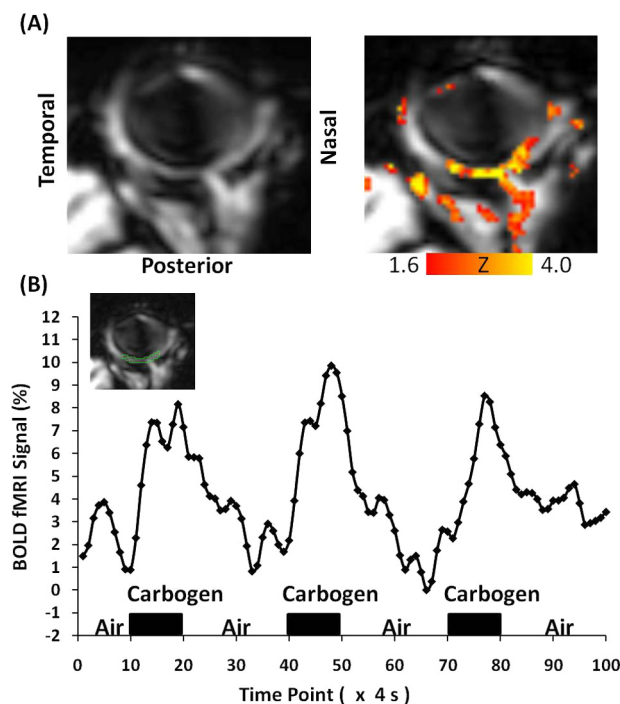


FIGURE 2. BOLD fMRI (A) color activation map and (B) time course associated with carbogen challenge from a representative subject.

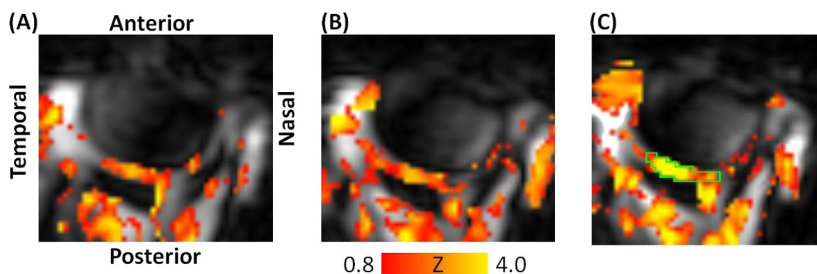


FIGURE 3. Reproducibility of BOLD fMRI color activation maps associated with carbogen challenge from three repeated trials of a same subject. ROI is overlaid on the activation map in (C).

vide a valuable tool to study neurovascular coupling, which may be perturbed in early disease states as demonstrated in many neurologic diseases. The utility of BOLD fMRI to image diseased retinas however remained to be demonstrated.

Choice of Pulse Sequence

Conventional gradient echo-planar imaging BOLD MRI yielded unacceptable quality in the human retina, including blurring, distortion, and signal dropout due to susceptibility artifacts because the eye is in close proximity to air-tissue interface. The PRESTO pulse sequence overcame these limitations while maintaining similar spatiotemporal resolution. PRESTO yielded relatively high BOLD contrast coupled with reasonably high temporal resolution by using a unique feature in which TE is longer than TR by acquiring the echo of the previous RF pulse.³⁵ This doubles the temporal resolution compared with a traditional gradient-recalled echo sequence, while maximizing BOLD contrast. In addition, an inversion recovery pre-pulse was applied to suppress the vitreous signal and to minimize the PVE on the retinal voxels, which was important for detecting small BOLD signal changes.

Drift and Movement Artifacts

High-resolution MRI of the human retina is susceptible to drift and movement artifacts for several reasons. First, the high-resolution imaging pulse sequence is more demanding on the magnetic field gradient, which can lead to temperature-induced frequency and signal drift. We confirmed on phantoms that our imaging protocol with identical parameters did not have significant hardware-related drift in MRI scans acquired over half an hour (data not shown). Second, the thin retina is bounded by the sclera and the vitreous, which have very different signal intensities than the retina, and misregistration of the time-series images can thus lead to significant signal intensity contaminations. Third, in the unanesthetized human, gross (including blinking) and saccadic eye movement could compromise time-series fMRI studies. Fortunately, eye move-

ment was effectively managed with eye fixation, synchronized blinks, and postprocessing image coregistration. To ensure the absence of movement artifacts, time-loop movies of the raw data and center-of-mass time courses were evaluated. Signal time courses were also evaluated to ensure no sudden jumps or significant drift. These precautions were necessary because signal contamination from either side of the retina due to misregistration would markedly affect signal intensities.

Partial Volume Effect

The PVE due to the thin retina can be significant because the retina is bounded by the vitreous and sclera, which have very different signal intensities from that of the retina. Future studies will need to improve spatial resolution and sensitivity to differentiate BOLD fMRI signal changes between the *retinal* and *choroidal* vasculature,^{24,30,31} a significant challenge for optically based imaging techniques and an active area of research. Nonetheless, the current spatial resolution is sufficient to measure BOLD fMRI signal changes across the entire retina-choroid thickness. Improving spatial resolution per se will also yield improved BOLD signal changes (i.e., detection sensitivity) because minimizing PVE with the vitreous and sclera—which should yield no significant BOLD responses—would improve BOLD percent changes.

Oxygen versus Carbogen BOLD Responses

The coupling of blood flow, oxygenation, and metabolism in the brain has been well described.³⁶⁻³⁸ There is also evidence of such coupling in the retina. For example, flickering light increases retinal and optic nerve head blood flow³⁹ and respiratory challenges with oxygen or carbogen modulate ocular blood flow and retinal oxygenation.⁴⁰ Visual stimulation also modulates optical absorption and scattering as detected by intrinsic optical imaging.⁴ Gas inhalation challenge²⁴ and visually evoked³² retinal BOLD fMRI responses in animal models have been also reported recently. Our BOLD fMRI findings in the unanesthetized human retina are in general agreement

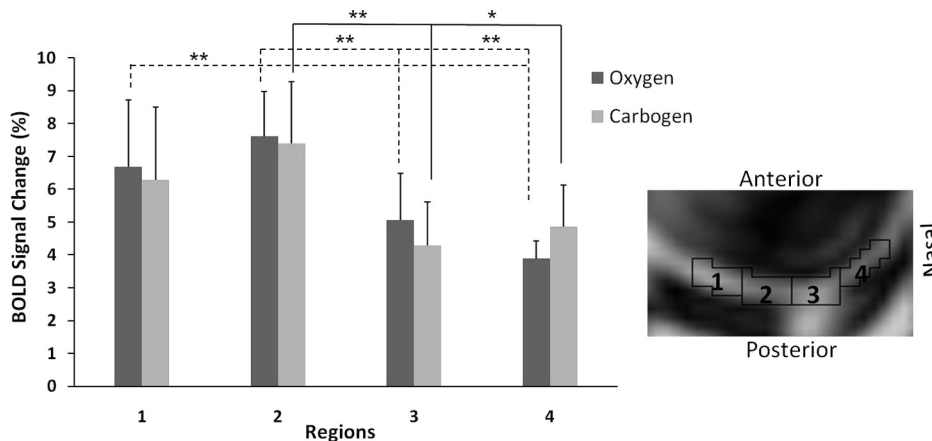


FIGURE 4. Regional BOLD signal changes from oxygen and carbogen challenges. ROIs are shown in the inset. Dashed lines indicate significant differences between ROIs from the oxygen challenge data, solid lines indicate significant differences between ROIs from carbogen challenge data. **P* < 0.05, ***P* < 0.01. Error bars, SD.

with previous studies showing strong vascular coupling in the retina.

Oxygen inhalation is expected to increase arteriole, capillary, and venous oxygen saturation and thus increase the BOLD signal relative to air inhalation, as has been well demonstrated in the brain.³⁶⁻³⁸ Oxygen inhalation has been reported to increase BOLD signals in the gray matter of the brain by 3.3% at 3 T,⁴¹ 3.41% at 1.5 T,⁴² and 1.7% at 1.5 T.⁴³ Note that BOLD signals are dependent on field strength, with higher field strength generally yielding larger changes. Blood flow through the choroid is high, and the arteriovenous oxygen difference in the choroid⁴⁴ is small compared with that in the brain. Thus, one might expect a small hyperoxia-induced BOLD increase. In contrast, the group-averaged BOLD increase in the retina-choroid during oxygen challenge was $5.2 \pm 1.4\%$, generally larger than those in the brain with good contrast-to-noise ratios. This is likely because the choroid has a high vascular density, and thus larger percent changes. In addition, it is worth pointing out that hyperoxia has a vasoconstrictive effect on the retinal vessels but not on choroidal vessels, and hyperoxia is known to markedly decrease retinal blood flow by 30–60% relative to air inhalation,^{9,45} compared with a 10% reduction in brain blood flow under hyperoxia.⁴⁶ Such vasoconstriction would tend to counteract the BOLD signal increase from elevated oxygen tension by hyperoxia per se. The net effect observed in our study is a positive BOLD increase, suggesting that the increased oxygen delivery per se from oxygen inhalation dominates. The results herein are consistent with a BOLD fMRI study of oxygen challenge reported in the rat retina, which also detected positive BOLD signal changes.²⁴ Laminar-specific BOLD and blood-flow measurements would help further explore these unique vascular responses in the retina and would have important applications.

Similarly, carbogen inhalation is expected to increase arteriole, capillary, and venous oxygen saturation and thus increase BOLD signal relative to air inhalation as has been well demonstrated in the brain.^{36,37} With the vasodilatory effect of 5% CO₂ in carbogen, BOLD responses are expected to be larger than for oxygen inhalation. Carbogen inhalation has been reported to increase BOLD signals in the gray matter of the brain by 3.6%,⁴³ and 6% at 1.5 T⁴⁷ and 6.8% at 2 T⁴⁸, which changes were indeed larger than those with oxygen inhalation in the brain described above. In the retina-choroid, the group-averaged BOLD percent changes to carbogen challenge was $5.2 \pm 1.3\%$, not statistically different from BOLD changes to oxygen challenge, contrary to predictions based on brain data. There are three possible explanations. First, although 5% CO₂ has significant vasodilatory effect on retinal vessels, it has little or no vasodilatory effect on choroid vessels,^{44,49,50} and the choroid is expected to dominate the BOLD responses because of its high vascular density.^{44,51} Second, the BOLD signal may have been near saturation with room air, and further vasodilation of the retinal vessels with carbogen and the small arteriovenous oxygen difference in the choroid would not further increase BOLD responses. Third, BOLD fMRI may not have sufficient sensitivity to detect the small BOLD differences between oxygen and carbogen inhalation, although this is unlikely if the magnitude of the changes is similar to those in the brain. The next logical step is to explore laminar-specific BOLD and blood-flow fMRI to address these and other questions and to further explore the unique hemodynamic and its regulation in the retina.

Some regional differences in BOLD fMRI responses in the retina were observed. The BOLD percent change was lower in region 3 (which included the optic nerve head) and higher in region 2 (which included the fovea). A possible explanation could be the sensitivity of the BOLD signals arising from different vessel types³⁷ and that the BOLD responses in the large

veins of the optic nerve head were small, compared with those in smaller vessels (capillaries and venules) in the fovea—that is, capillaries and venules were more deoxygenated compared with large veins under baseline. These regional differences, however, need to be interpreted with caution because of significant PVE, SNR limitation, and small sample size. Further studies are needed to investigate regional differences at higher spatial resolution.

Future Perspectives

Abnormal baseline oxygen tension and oxygenation responses to physiological challenges and visual stimulations have been implicated in many neurologic diseases. It would not be surprising that this would also be the case in retinal diseases, but this potential imaging biomarker has not been widely explored in the retina. Indeed, perturbed tissue oxygen tension in diabetic cat retinas has been reported with oxygen electrodes.⁵² Oxygen tension based on the phosphorescent quenching by oxygen showed abnormal retinal vascular oxygen tension responses to light flicker in diabetic rats, suggesting impaired increases in oxygen consumption normally provoked by light flicker.⁵³ Given the lack of depth-resolved, physiological imaging techniques and the challenges in obtaining quantitative blood flow data in the in vivo retinas, MRI approaches to image retinal physiology and function in responses to challenges and visual stimulations warrant further investigation.

Future studies will aim at improving spatial resolution sufficiently to achieve laminar resolution and then explore the unique hemodynamic regulation in the retina. Laminar resolution of BOLD,²⁴ blood-volume,³¹ and blood-flow³⁰ fMRI methodologies are feasible in animal models. Translating these MRI methodologies that are already widely used for brain studies to image the unanesthetized human retina could have important applications. These applications may include staging and diagnosis of retinal diseases, monitoring of therapeutic intervention, and testing novel therapeutic strategies.

References

1. Fujimoto JG, Brezinski ME, Tearney GJ, et al. Optical biopsy and imaging using optical coherence tomography. *Nat Med.* 1995;1:970–972.
2. Shonat RD, Richmond KN, Johnson PC. Phosphorescence quenching and the microcirculation: an automated, multipoint oxygen tension measuring instrument. *Rev Sci Instrum.* 1995;66:5075–5084.
3. Tsunoda K, Oguchi Y, Hanazono G, Tanifuji M. Mapping cone- and rod-induced retinal responsiveness in macaque retina by optical imaging. *Invest Ophthalmol Vis Sci.* 2004;45:3820–3826.
4. Grinvald A, Bonhoeffer T, Vanzetta I, et al. High-resolution functional optical imaging: from the neocortex to the eye. *Ophthalmol Clin N Am.* 2004;17:53–67.
5. Tso DY, Schallek J, Zarella M, et al. Pharmacological dissection of laminar contributions to intrinsic optical signals in the retina. *Assoc Res Vis Ophthalmol.* 2006;5899.
6. Preussner PR, Richard G, Darrelmann O, Weber J, Kreissig I. Quantitative measurement of retinal blood flow in human beings by application of digital image-processing methods to television fluorescein angiograms. *Graefes Arch Clin Exp Ophthalmol.* 1983;221:110–112.
7. Guyer DR, Yannuzzi LA, Slakter JS, Sorenson JA, Orlock S. The status of indocyanine-green videoangiography. *Curr Opin Ophthalmol.* 1993;4:3–6.
8. Wajer SD, Taomoto M, McLeod DS, et al. Velocity measurements of normal and sickle red blood cells in the rat retinal and choroidal vasculatures. *Microvasc Res.* 2000;60:281–293.
9. Riva CE, Grunwald JE, Singclair SH. Laser Doppler velocimetry study of the effect of pure oxygen breathing on retinal blood flow. *Invest Ophthalmol Vis Sci.* 1983;24:47–51.

10. Riva CE, Harino S, Petrig BL, Shonat RD. Laser Doppler flowmetry in the optic nerve. *Exp Eye Res.* 1992;55:499-506.
11. Riva CE, Cranstoun SD, Mann RM, Barnes GE. Local choroidal blood flow in the cat by laser Doppler flowmetry. *Invest Ophthalmol Vis Sci.* 1994;35:608-618.
12. Cheng H, Duong TQ. Simplified laser-speckle-imaging analysis method and its application to retinal blood flow imaging. *Opt Lett.* 2007;32:2188-2190.
13. Cheng H, Yan Y, Duong TQ. Temporal statistical analysis of laser speckle image and its application to retinal blood-flow imaging. *Opt Express.* 2008;16:10214-10219.
14. Riva CE, Petrig BL. Choroidal blood flow by laser Doppler flowmetry. *Opt Eng.* 1995;34:746-752.
15. Riva CE, Falsini B. Functional laser Doppler flowmetry of the optic nerve: physiological aspects and clinical applications. *Prog Brain Res.* 2008;173:149-163.
16. Ugurbil K, Adriany G, Andersen P, et al. Magnetic resonance studies of brain function and neurochemistry. *Annu Rev Biomed.* 2000;2:633-660.
17. Ogawa S, Lee T-M, Kay AR, Tank DW. Brain magnetic resonance imaging with contrast dependent on blood oxygenation. *Proc Natl Acad Sci USA.* 1990;87:9868-9872.
18. Kim D-S, Duong TQ, Kim S-G. High-resolution mapping of iso-orientation columns by fMRI. *Nature Neurosci.* 2000;3:164-169.
19. Duong TQ, Kim D-S, Ugurbil K, Kim S-G. Localized blood flow response at sub-millimeter columnar resolution. *Proc Natl Acad Sci USA.* 2001;98:10904-10909.
20. Cheng K, Waggoner RA, Tanaka K. Human ocular dominance columns as revealed by high-field functional magnetic resonance imaging. *Neuron.* 2001;32:359-397.
21. Silva AC, Koretsky AP. Laminar specificity of functional MRI onset times during somatosensory stimulation in rat. *Proc Natl Acad Sci USA.* 2002;99:15182-15187.
22. Goense JB, Logothetis NK. Laminar specificity in monkey V1 using high-resolution SE-fMRI. *Magn Reson Imag.* 2006;24:381-392.
23. Shen Q, Cheng H, Pardue MT, et al. Magnetic resonance imaging of tissue and vascular layers in the cat retina. *J Magn Reson Imag.* 2006;23:465-472.
24. Cheng H, Nair G, Walker TA, et al. Structural and functional MRI reveals multiple retinal layers. *Proc Natl Acad Sci USA.* 2006;103:17525-17530.
25. Chen J, Wang Q, Zhang H, et al. In vivo quantification of T(1), T(2), and apparent diffusion coefficient in the mouse retina at 11.74T. *Magn Reson Med.* 2008;59:731-738.
26. Nair G, Shen Q, Duong TQ. Relaxation time constants and apparent diffusion coefficients of rat retina at 7 tesla. *Int J Imag Sys Tech.* 2010;20:126-130.
27. Nair G, Cheng H, Kim M, et al. Manganese-enhanced MRI reveals multiple cellular and vascular layers in normal and degenerated retinas. *Proc Int Soc Magn Reson Med.* 2007:2452.
28. Li Y, Cheng H, Duong TQ. Blood-flow magnetic resonance imaging of the retina. *Neuroimage.* 2008;39:1744-1751.
29. Li Y, Cheng H, Shen Q, et al. Blood-flow magnetic resonance imaging of retinal degeneration. *Invest Ophthalmol Vis Sci.* 2009;50:1824-1830.
30. Muir ER, Duong TQ. MRI of retinal and choroidal blood flow with laminar resolution. *NMR Biomed.* Epub ahead of print September 6, 2010.
31. Nair G, Tanaka Y, Pardue MT, Olson DE, Thule PM, Duong TQ. MRI reveals differential regulation of retinal and choroidal blood volume in rat retina. *Neuroimage.* Epub ahead of print September 17, 2010.
32. Duong TQ, Ngan S-C, Ugurbil K, Kim S-G. Functional magnetic resonance imaging of the retina. *Invest Ophthalmol Vis Sci.* 2002;43:1176-1181.
33. Richdale K, Wassenaar P, Teal Bluestein K, et al. 7 tesla MR imaging of the human eye in vivo. *J Magn Reson Imaging.* 2009;30:924-932.
34. Alsop DC, Maldjian JA, Detre JA. In vivo MR perfusion imaging of the human retina. *Internat Soc Magn Reson Med.* 2000;162.
35. Liu G, Sobering G, Duyn J, Moonen CTW. A functional MRI technique combining principles of echo-shifting with a train of observations (PRESTO). *Magn Reson Med.* 1993;30:764-768.
36. Raichle ME. Circulatory and metabolic correlates of brain function in normal humans. In: Plum F, ed. *Handbook of Physiology—The Nervous System V: Higher Functions of the Brain.* Bethesda: American Physiological Society; 1987:643-674.
37. Buxton RB, Frank LR. A model for the coupling between cerebral blood flow and oxygen metabolism during neural stimulation. *J Cereb Blood Flow Metab.* 1997;17:64-72.
38. Hoge RD, Atkinson J, Gill B, Crelier GR, Marrett S, Pike GB. Linear coupling between cerebral blood flow and oxygen consumption in activated human cortex. *Proc Natl Acad Sci.* 1999;96:9403-9408.
39. Riva CE, Harino S, Shonat RD, Petrig BL. Flicker evoked increase in optic nerve head blood flow in anesthetized cats. *Neurosci Lett.* 1991;128:291-296.
40. Yu D-Y, Cringle SJ. Oxygen distribution and consumption within the retina in vascularised and avascular retinas and in the animal models of retinal disease. *Prog in Retinal Eye Res.* 2001;20:175-208.
41. Chiarelli PA, Bulte DP, Wise R, Gallichan D, Jezzard P. A calibration method for quantitative BOLD fMRI based on hyperoxia. *Neuroimage.* 2007;37:808-820.
42. Losert C, Peller M, Schneider P, Reiser M. Oxygen-enhanced MRI of the brain. *Magn Reson Med.* 2002;48:271-277.
43. Macey PM, Alger JR, Kumar R, Macey KE, Woo MA, Harper RM. Global BOLD MRI changes to ventilatory challenges in congenital central hypoventilation syndrome. *Respir Physiol Neurobiol.* 2003;139:41-50.
44. Bill A. Circulation in the eye. In: Renkin EM, Michel CC, eds. *Handbook of Physiology, Microcirculation Part 2.* Bethesda, MD: American Physiological Society; 1984:1001-1035.
45. Trokel S. Effect of respiratory gases upon choroidal hemodynamics. *Arch Ophthalmol.* 1965;73:838-842.
46. Kety SS, Schmidt CF. The effects of altered arterial tensions of carbon dioxide and oxygen on cerebral blood flow and cerebral oxygen consumption of normal young men. *J Clin Invest.* 1948;27:484-491.
47. Rauscher A, Sedlacik J, Barth M, Haacke EM, Reichenbach JR. Noninvasive assessment of vascular architecture and function during modulated blood oxygenation using susceptibility weighted magnetic resonance imaging. *Magn Reson Med.* 2005;54:87-95.
48. Rostrup E, Larsson HBW, Toft PB, et al. Functional MRI of CO₂ induced increase in cerebral perfusion. *NMR Biomed.* 1994;7:29-34.
49. Roth S. The effects of halothane on retinal and choroidal blood flow in cats. *Anesthesiology.* 1992;76:455-460.
50. Tilton RG, Chang K, Weigel C, et al. Increased ocular blood flow and 125I-albumin permeation in galactose-fed rats: inhibition by sorbinil. *Invest Ophthalmol Vis Sci.* 1988;29:861-868.
51. Geiser MH, Riva CE, Dorner GT, Diermann U, Luksch A, Schmetterer L. Response of choroidal blood flow in the foveal region to peroxia and hyperoxia-hypercapnia. *Curr Eye Res.* 2000;21:669-676.
52. Linsenmeier RA, Braun RD, McRipley MA, et al. Retinal hypoxia in long-term diabetic cats. *Invest Ophthalmol Vis Sci.* 1998;39:1647-1657.
53. Blair NP, Wanek JM, Mori M, Shahidi M. Abnormal retinal vascular oxygen tension response to light flicker in diabetic rats. *Invest Ophthalmol Vis Sci.* 2009;50:5444-5448.